Active Disturbance Rejection Control for PMLM Servo System in CNC Machining*

GUO Jianxin · XUE Wenchao · HU Tao

DOI: 10.1007/s11424-015-3258-2
Received: 30 October 2013 / Revised: 4 May 2015

Abstract Uncertain friction is a key factor that influences the accuracy of servo system in CNC machine. In this paper, based on the principle of Active Disturbance Rejection Control (ADRC), a control method is proposed, where both the extended state observer (ESO) and the reduced order extended state observer (RESO) are used to estimate and compensate for the disturbance. The authors prove that both approaches ensure high accuracy in theory, and give the criterion for parameters selection. The authors also prove that ADRC with RESO performs better than that with ESO both in disturbance estimation and tracking error. The simulation results on CNC machine show the effectiveness and feasibility of our control approaches.

Keywords Active disturbance rejection control, CNC machine, nonlinear friction, parameter selection, servo system.

1 Introduction

With the development of the mechanical manufacturing technology, permanent magnet synchronous motor (PMLM) gradually becomes one of the most competitive motion control products with high speed, high precision, high efficiency, which has been widely utilized in domain such as NC milling machine, cutting machine tool, lathe or high-grade CNC machine tools[1]. Due to the linear construction, PMLM motor has an incomparable advantage compared with rotating motor. One of the most important points is that middle mechanical drive conversion link is saved so as to realize the feeding system "zero transmission", to improve the system transmission stiffness and to reduce the mechanical wear substantially. Moreover, it possesses higher speed and higher acceleration or deceleration ability. As is known, high speed cutting

GUO Jianxin · XUE Wenchao · HU Tao
Key Laboratory of Mathematics Mechanization, Academy of Mathematic and Systems Science, Chinese Academy of Sciences, Beijing 100190, *China*; *Key Laboratory of Systems and Control, Academy of Mathematics and Systems Science, Chinese Academy of Sciences, Beijing* 100190, *China*. Email: wenchaoxue@amss.ac.cn.
*This paper was partially supported by the National Key Basic Research Project of China under Grant No. 2011CB302400, the National Basic Research Program of China under Grant No. 2014CB845303 and the National Center for Mathematics and Interdisciplinary Sciences, Chinese Academy of Sciences.
◇ *This paper was recommended for publication by Editor HONG Yiguang.*

can significantly improve the metal processing precision, surface processing quality and production efficiency as well as the service life of CNC machine tools, by the virtue of which PMLM can meet the needs of high speed and high precision processing. So it is of great significance in high-end CNC machine[2].

Although the linear motor has many advantages compared with the rotating motor, the linear motor control system also claims higher requirements. The mathematical model of PMLM is a multi-variable, nonlinear system[3], which makes it difficult to utilize traditional controller. With the development of research of the control theory and linear motor, many scholars put forward various methods from classical control to modern control, such as PID control, adaptive control, self-learning control[4–6], and so forth. Nevertheless, these control methods have a variety of limitations, which either rely too much on accurate mathematical model or narrow scope of robustness. Hence, a better quality, higher efficiency and more practical control algorithm are the primary issues in need of solution.

The Active Disturbances Rejection Control (ADRC) is a new control method which does not depend on the accurate mathematical model of the plant. Through improving the classic PID inherent defects, the controller algorithm is simple, and the parameters of the scope is adaptable. Since ADRC can utilize the extended state observer to estimate the total disturbance including the internal and external disturbance of the plant, it can ensure the system to generate ideal control effect, perform stronger robustness of maneuverability. These virtues attract much attention both in theory (see [7–9]) and application (see [10–12]).

In this paper, in order to ensure the accuracy in manufacture process, we apply the ADRC control method to PMLM mounted in CNC motion system with complicated nonlinear part. We use series square wave to simulate the unspecific part aiming to approximate practical situation to a great extend. Moreover, ESO used in ADRC is replaced via reduced order ESO (RESO), the reason for which is that the measured output does not need to be estimated. Comparisons are presented to verify the effectiveness of ESO and RESO as well. We also obtain the relationship between the parameters of ESO (and RESO) and tracking performance. In addition, the theoretical results help to offer the reference for us to select the parameters of ESO (and RESO) reasonably in practice. An example from CNC is used to test the approach in the end.

The paper is organized as follows. The model of the motor and the motion control problem are introduced in Section 2. The general principle and structure of the ADRC are presented in Section 3. Stability analysis and parameters tuning method are discussed in Section 4. Simulation test is shown in Section 5. Finally, some concluding remarks are given in Section 6.

2 Modeling the PMLM Motor

In order to describe the proposed servo control scheme, the voltage controllable PMLM is adopted, whose mechanical dynamics and circuit dynamics are expressed as the following forces balance equation[13]

$$M\ddot{x}_1 + D\dot{x}_1 + F_d = K_f i(t) \tag{1}$$

and the voltage balance equation

$$K_e\dot{x}_1 + L\dot{i} + Ri = u(t), \tag{2}$$

where x_1 is the motion position, $\dot{x}_1 = \frac{dx_1}{dt}$, and the parameters have the following meaning:

M is the moving thrust block mass,

D is the viscious coefficient;

F_d is the load force;

K_f is the amount of force produced by the motor;

$i(t)$ is the armature current;

K_e is the back EMF voltage;

L is the electrical constant parameter;

R is the armature resistance;

$u(t)$ is the armature voltage.

In this paper, the load force is assumed to be composed of three parts: The external load force which is bounded, the ripple force arising from the magnetic structure of the PMLM and other physical imperfections, and the frictional force[14, 15]. So the total load force can be described as

$$F_d = F_{\text{load}} + F_{\text{fric}} + F_{\text{ripple}},$$

where F_{load}, F_{fric}, and F_{ripple} are the external load force, friction force, and ripple force respectively. We assume

$$|F_{\text{load}}(t)| \leq F_{lM}, \quad t > 0$$

and the friction is assumed to be

$$F_{\text{fric}} = (F_c + (F_s - F_c)\mathrm{e}^{-(\frac{\dot{x}_1}{x_s})^2} + F_v\,|\dot{x}_1|)\text{sign}(\dot{x}_1),$$

where F_c is the Coulomb friction, F_s is the static friction force, F_v is the viscous friction coefficient, and x_s is the lubrication coefficient. The last part of the friction is a significant disturbance from the uniform magnetic field of the permanent magnet and other physical imperfections in the process of linear driver. These factors could be represented as the wave power to ripple, which often can be written in the form of trigonometric functions of the load position. In reality, the ripple force is more complex due to variations in the magnet dimension, but it has a comparable period and amplitude as described in [15]. So, we have

$$F_{\text{ripple}} = A_r \sin(\omega x_1 + \phi),$$

where A_r, ω, ϕ are constant parameters. Additionally, all the parameters introduced above can be obtained through experiments and can be regarded as constants.

Finally, since the electrical time constant parameter L is much smaller than the mechanical ones, the delay of electrical response can be ignored and we obtain a second order system from (1) and (2)

$$\ddot{x}_1 = -\frac{1}{M}\left(\frac{K_f K_e}{R} + D\right)\dot{x}_1 - \frac{F_d}{M} + \frac{K_f u(t)}{MR}.$$

Regarding the current as the internal disturbance and defining $a_1 = \frac{1}{M}(\frac{K_f K_e}{R} + D)$, $b_0 = \frac{K_f}{MR}$ and $f_d(\dot{x}_1, x_1, w(t)) = \frac{F_d}{M}$, the above equation can be written as

$$\ddot{x}_1 = -a_1\dot{x}_1 - f_d + b_0 u(t).$$

Define $x_2 = \dot{x}_1$. Hence we obtain the state equation of the system

$$\begin{cases} \dot{x}_1 = x_2, \\ \dot{x}_2 = x_3 + b_0 u, \\ y = x_1, \end{cases} \tag{3}$$

where

$$x_3 = -a_1 x_2 - f_d.$$

In the frame of ADRC, x_3 is regard as the "total disturbance" which lumps the external and the internal disturbance of the system.

Note that f_d can be written as $f_d = f_v x_2 + f_0$, $f_v = \frac{F_v}{M}$, $f_0 = \frac{1}{M}[F_{\text{load}} + F_{\text{ripple}} + (F_c + (F_s - F_c)\mathrm{e}^{-(\frac{x_2}{x_s})^2})\text{sign}(x_2)]$ and f_0 is bounded.

3 ADRC Designs with ESO and RESO

In this section, we give an ADRC based control for PMLM, which consists of an ESO and a linear form in NLSEF part. Since the derivatives of the signals are known, TD is not used. General form about the design of ADRC can be referred to [16].

For the PMLM system (5), the ESO for PMLM has the following form

$$\begin{cases} \dot{\widehat{x}}_1 = \widehat{x}_2 - \beta_1(\widehat{x}_1 - y), \\ \dot{\widehat{x}}_2 = \widehat{x}_3 - \beta_2(\widehat{x}_1 - y) + b_0 u, \\ \dot{\widehat{x}}_3 = -\beta_3(\widehat{x}_1 - y), \end{cases} \tag{4}$$

where $\beta_1, \beta_2, \beta_3$ are determined by the ESO-bandwidth ω as follows $\beta_1 = 3\omega$, $\beta_2 = 3\omega^2$, $\beta_3 = \omega^3$.

In this paper, the following linear form is used in the place of NLSEF

$$u_0 = k_p(v - \widehat{x}_1) + k_d(\dot{v} - \widehat{x}_2) + \ddot{v}, \tag{5}$$

where v stands for the reference input signal, and k_p, k_d are determined by the controller bandwidth ω_c as follows: $k_p = \omega_c^2, k_d = 2\omega_c$.

There are two reasons for using the above linear form feedback. First, the controller structure is simple to be implemented in practice. Second, a large number of application studies indicate that the linear feedback structure can also perform well to cope with the nonlinear uncertainties[8, 9, 17]. Thus, the corresponding controller is

$$u = \frac{u_0 - \widehat{x}_3}{b_0}, \tag{6}$$

which will be used to implement the control in PMLM system (5).

Since the output of the system $y = x_1$ can be directly measured, it is unnecessary to estimate x_1 by $\widehat{x}_1$. According to the reduced order state observer (RESO) in [18], we can design the following RESO for the PMLM system (5) as follows:

$$\begin{cases} \begin{pmatrix} \dot{\widehat{v}}_2 \\ \dot{\widehat{v}}_3 \end{pmatrix} = \begin{pmatrix} -\beta_1 & 1 \\ -\beta_2 & 0 \end{pmatrix} \begin{pmatrix} \widehat{v}_2 \\ \widehat{v}_3 \end{pmatrix} + \begin{pmatrix} -\beta_1 & 1 \\ -\beta_2 & 0 \end{pmatrix} x_1 + \begin{pmatrix} 1 \\ 0 \end{pmatrix} b_0 u, \\ \begin{pmatrix} \widehat{x}_2 \\ \widehat{x}_3 \end{pmatrix} = \begin{pmatrix} \widehat{v}_2 \\ \widehat{v}_3 \end{pmatrix} + \begin{pmatrix} \beta_1 \\ \beta_2 \end{pmatrix} x_1. \end{cases} \tag{7}$$

Similar to the situation of ESO, β_1, β_2 are determined by RESO bandwidth ω: $\beta_1 = 2\omega, \beta_2 = \omega^2$. Thus, the following RESO controller for the PMLM system (5) is obtained:

$$\begin{cases} u = \dfrac{u_0 - \widehat{x}_3}{b_0}, \\ u_0 = k_p(v - x_1) + k_d(\dot{v} - \widehat{x}_2) + \ddot{v}, \end{cases} \tag{8}$$

where k_p, k_d are determined by the controller bandwidth ω_c: $k_p = \omega_c^2, k_d = 2\omega_c$.

4 Stability and Boundary Analysis

In this section we aim to analyze the stability of the ADRC in PMLM. Based on the work in [19], we further analyze performances of the closed-loop which adopt the stratagy of ESO and RESO, respectively. Moreover, we prove that ADRC with RESO performs better than that with ESO both in tracking error and disturbance estimation.

For the load $F_{\text{load}}(t)$ and the reference signal v, we make the assumption as follows.

Assumption 1 $|F_{\text{load}}(t)| \leq F_{lM} < \infty, t > 0$, piecewise continuous, and only posses discontinuity point of the first kind $\{t_i\}_{i=1}^{\infty}$, $t_{i-1} < t_i$, and $\inf_i \{t_i - t_{i-1}\} > 0$; $F_{\text{load}}(t)$ is derivable on (t_{i-1}, t_i), $i = 1, 2, \cdots$, and the derivative is bounded as well.

Assumption 2 The reference position signal v and the velocity signal $\dot{v}$ are continuously differentiable. Besides, v and $\dot{v}$ are bounded.

For simplication, we ignore the Coulomb friction and the static friction in the friction model. So in the system (5), f_d reduces to $f_d = f_0 + f_v x_2$, where

$$f_0 = \frac{1}{M}(F_{\text{load}} + F_{\text{ripple}}). \tag{9}$$

Define $x^* = (x_1^*, x_2^*)^{\mathrm{T}}$,

$$\begin{aligned} \dot{x}_1^* &= x_2^*, \\ \dot{x}_2^* &= \ddot{v} - k_p(x_1^* - v) - k_d(x_2^* - \dot{v}). \end{aligned} \tag{10}$$

Here, the initial value of x^* are $x_1^*(t_0) = x_1(t_0)$, $x_2^*(t_0) = x_2(t_0)$. We will show that the states (x_1, x_2) of the closed-loop system of ADRC can be closed to the (x_1^*, x_2^*) for $t \in [t_0, \infty)$. Besides, for convenience, we denote $\widetilde{x} = (\widetilde{x}_1, \widetilde{x}_2)^{\mathrm{T}} = (x_1 - x_1^*, x_2 - x_2^*)^{\mathrm{T}}$, $\overline{e} = (\overline{e}_1, \overline{e}_2, \overline{e}_3)^{\mathrm{T}} = (\widehat{x}_1 - x_1, \widehat{x}_2 - x_2, \widehat{x}_3 - x_3)^{\mathrm{T}}$.

Theorem 4.1 *Based on Assumptions* 1 *and* 2, (5) *ensures the closed-loop possessing the following properties: When* ω *is large enough,*

$$\|\overline{e}(t)\| \leq \overline{T}_1 \cdot \frac{1}{\omega}, \quad t \in \left[t_{i-1} + 2\overline{c}_{22}\frac{\ln\omega}{\omega}, t_i\right), \tag{11}$$

$$\|\widetilde{x}\| \leq \overline{T}_2 \cdot \frac{\ln\omega}{\omega}, \quad t \in [t_0, \infty), \tag{12}$$

where $\overline{c}_{22} = 4.3372$, $\overline{T}_1$ *and* $\overline{T}_2$ *are positives depending on* ω_c, *the initial values, uncertainty, and the reference signals.*

The corresponding proof is in the appendix B. From the analysis above, we can draw the conclusions:

1) (11) ensures that $\widehat{x}_1$, $\widehat{x}_2$ and $\widehat{x}_3$ can track x_1, x_2 and x_3 fast, so that the disturbance estimation is smaller in the sections out of the removable points. Moreover, the disturbance estimation error can be adjusted via ω. In addition, from the proof in Appendix B, we get $\overline{T}_1 = \frac{\overline{c}_{22}}{\overline{c}_{21}}\overline{s}_4 + \frac{\sqrt{\overline{c}_{22}}}{\sqrt{\overline{c}_{21}}}\overline{\rho}_3$, where $\overline{s}_4$ and $\overline{\rho}_3$ are positive constants related to the initial values, uncertainty and the reference signal's bound. Thus, we get that the larger bound of the uncertainty, the larger ω required to achieve estimation.

2) (12) indicates that the smaller error will be between $x(t)$ and $x^*(t)$. Viewed from the proof in Appendix B, we get $\overline{T}_2 = \frac{4\overline{c}_{22}\overline{\rho}_3 r_1(\omega_c)}{\overline{c}_{11}} \cdot \frac{\mathrm{e}^{\frac{\delta_t}{\overline{c}_{12}}}}{\mathrm{e}^{\frac{\delta_t}{2\overline{c}_{12}}}-1}$, where $\overline{\rho}_3$ is a positive constant related to the initial values, uncertainty and the reference signal's bound and $r_1(\omega_c)$ is a decreasing function with respect to ω_c. Thus, we get that the larger ω or ω_c, the better tracking effect will be obtained.

The skill used in the proof of the ESO is similar to that of RESO, which is only different from the other in the order and small change in parameters. Besides, define $\widetilde{x} = (\widetilde{x}_1, \widetilde{x}_2)^{\mathrm{T}} = (x_1 - x_1^*, x_2 - x_2^*)^{\mathrm{T}}$, $\widehat{e} = (\widehat{e}_2, \widehat{e}_3)^{\mathrm{T}} = (\widehat{x}_2 - x_2, \widehat{x}_3 - x_3)^{\mathrm{T}}$. Hence, the closed-loop system of PMLM using ADRC with RESO can be described as follows.

Theorem 4.2 *Based on Assumptions* 1 *and* 2, (8) *ensures the following properties: When* ω *is large enough,*

$$\|\widehat{e}(t)\| \leq T_1 \cdot \frac{1}{\omega}, \quad t \in \left[t_{i-1} + 2c_{22}\frac{\ln\omega}{\omega}, t_i\right), \tag{13}$$

$$\|\widetilde{x}\| \leq T_2 \cdot \frac{\ln\omega}{\omega}, \quad t \in [t_0, \infty), \tag{14}$$

where $c_{22} = 1.7071$, T_1 *and* T_2 *are positives depending on* ω_c, *the initial values, uncertainty, and the reference signals.*

The corresponding proof is in Appendix A. Similar to the case in Theorem 4.1, we get that

1) (13) confirms that the higher estimation can be achieved through selecting the larger ω especially when the bound of the uncertainty is considered.

2) Besides, from (14), smaller tracking error, i.e., the difference between $x(t)$ and $x^*(t)$, will be obtained via the monotonous selecting larger parameter ω or ω_c.

Remark 4.3 In the light of the proof of Theorems 4.1 and 4.2, we can make a comparison between ESO and RESO if we choose the same parameters ω_c, ω and the same initial values:

1) Since $\overline{c}_{22} = 4.3372 > c_{22} = 1.7071$, comparison between (11) and (13) shows

$$\overline{t}_i^* > t_i^*, \quad i = 0, 1, \cdots, \tag{15}$$

which revels that, in the discontinuous points compared with ESO, RESO can estimate the disturbance faster;

2) According to the proof in Appendix C, we can see that $T_1 \leq \overline{T_1}$ and $T_2 \leq \overline{T_2}$. Therefore, compared with ESO, the estimation error $\|\widehat{e}\|$ is much smaller under RESO. In addition, the tracking error $\|\widetilde{x}\|$ is smaller under RESO as well.

In the next section, simulation will be implemented to further investigate the control effect between ESO and RESO.

5 CNC Machining Based on ADRC

The motion planning of computer numerical control (CNC) manufacturing systems can be divided into three main courses: Path planning, trajectory generation and trajectory tracking. The path planning consists of determining a geometric path according to the specified task. The desired curve $\vec{r}(u) = (x(u), y(u))$ (u is curve parameter) is generated from a solid modeler, the process of which is also named as CAM (Computer Aided Manufacturing)[20]. In the trajectory generation process, kinematic bounds information, such as velocity, acceleration, and jerk (derivative of acceleration with respect to time), are determined, after which the interpolator which calculates the intermediate coordinates using an appropriate interpolation algorithm[21–24]. Due to the function of the interpolator relating the parameter u (the curve parameter) and time t, the description of the trajectory can be used in the control system. Such a relationship can be determined if the feedrate specifications are known. Feedrate will be determined through optimization with considering the kinematic information determined at the beginning, and it can be a constant or variable throughout the path. Given a feedrate profile $v_f(t)$, it is possible to obtain the desired coordinates as a function of time

$$v_f(t) = \sqrt{\left(\frac{dx(u)}{dt}\right)^2 + \left(\frac{dy(u)}{dt}\right)^2} = \frac{du}{dt}\sqrt{x'(u)^2 + y'(u)^2},$$

where $(\cdot)' = \frac{d}{du}(\cdot)$.

Since the feedrate is assumed to be known, we have a differential equation between u and t

$$\frac{du}{dt} = \frac{v_f(t)}{\sqrt{x'(u)^2 + y'(u)^2}}.$$

Using this differential equation, the command signal is now available as a function of time. It is also possible to find the time derivative of the command for control purposes. Finally, it is easy to implement trajectory tracking process using the closed-loop controllers to regulate the actuators moving along the planned trajectory. The basic system consists of two motors, each

motor moving the tool along a single axis of motion. In the simulation below, we apply PMLM motor to act as the axis drive motor. ESO and RESO are mounted on ADRC, respectively. The overall system for ESO case is illustrated in Figure 1.

Table 1 Parameters used in the simulation

Meaning	Parameter	Unit	Value
Mass of thrust block	M	Kg	5.4
Viscosity constant	D	Ns/m	10
Armature resistance	R	Ohms	16.8
Armature inductance	L	Henry	17.4×10^{-3}
electrical-mechanical energy conversion constant	K_f	N/A	130
back electromotive force (EMF) voltage	K_e	v/m/s	123
Minimum level of coulomb friction	f_c	Newton	10
Static friction	f_s	Newton	20
Viscous friction parameter	f_v	Newton	10
Ripple paremeter 1	A_r	Newton	8.5
Ripple patemeter 2	ω	Rad/m	314
Ripple patemeter 3	φ	unit	0.05π
Bounded force	f_{lm}	Newton	100
Viscous parameter	x_s	m/s	0.1

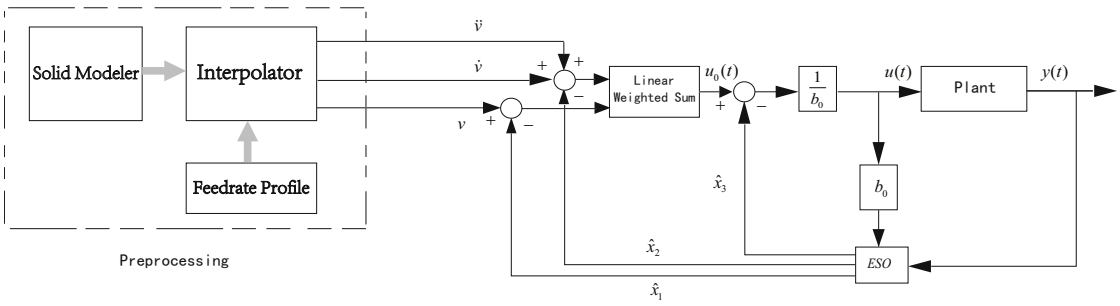

Figure 1 Overall system

Figure 2 is a butterfly curved segments[25] generated from the solid modeler of the CNC system.

There is a lot of velocity planning methods. In this paper, a quintic splines trajectory generation algorithm[26] is utilized to connect a series of reference knots that produces continuous position, feedrate optimization technique in [27] for minimizing the cycle time in machining spline tool paths with axis velocity, acceleration and jerk limits. The plane butterfly curve is discretized to more than 100 points which are close enough to be the reference knots. The drive constraints are set to be $\vec{V}_{\max} = (200, 200)\text{mm/s}$, $\vec{A}_{\max} = (4000, 4000)\text{mm/s}^2$,

$\vec{J}_{\max} = (50000, 50000)\text{mm/s}^3$. The initial and terminal velocities and accelerations are all zero, and we set the initial position of the curve at origin points (0, 0); the sampling period is set to be 1ms and the same physical parameters are assumed for both the x and y axes; the parameters of PMLM are given in the Table 1. Especially, F_{load} is simulated as a piece constants, the period of which is 3s with eighties percents of the periods being constant value 50 and the rest being value 100. Simulation is carried out to make comparison between ESO and RESO which are applied in ADRC by using Matlab/Simulink. The control bandwidth and the bandwidth for the simulation is ω_c=800 and ω =1000, which are adjusted under the guidance from the theorem discussed in Section 4. The effects are demonstrated in the following figures.

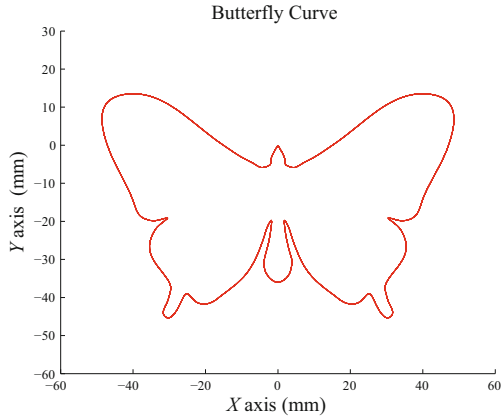

Figure 2 The reference knots and cubic spline trajectory

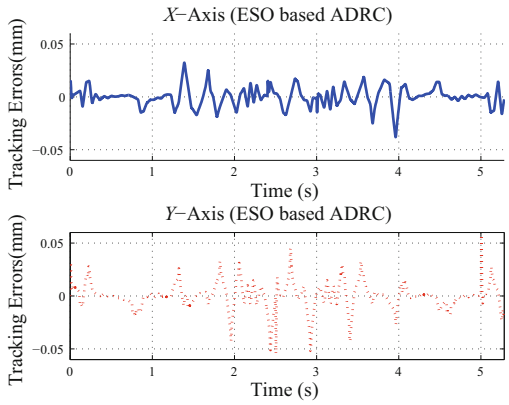

Figure 3 Tracking error of ESO-ADRC

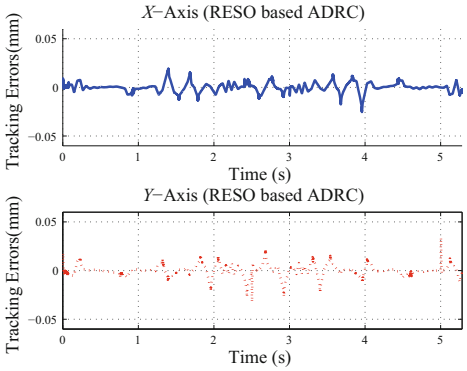

Figure 4 Tracking error of RESO-ADRC

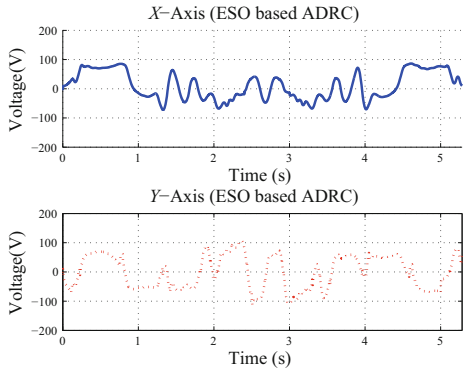

Figure 5 Voltage of ESO-ADRC

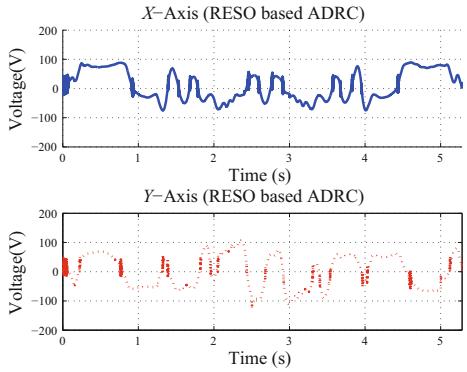

Figure 6 Voltage of RESO-ADRC

Figures 3 and 4 are the tracking error comparison. As can be seen from the picture, if we define mean error $e_{\text{mean}} = (\sum_{i=1}^{N} |e_i|)/N$ to demonstrate average accuracy in the total progress, where N denotes the number of the interpolation points, then the corresponding axis average

accuracy for the two method are $\vec{e}_{\text{mean}}^{\text{ESO}} = (0.0060, 0.0079)\text{mm}$ and $\vec{e}_{\text{mean}}^{\text{RESO}} = (0.0032, 0.0038)\text{mm}$, respectively. Thus, the error generated by ESO is larger than that of RESO, at the cost of a small vibration of the control voltage (near zeros in the horizontal axis) which is shown in Figures 5 and 6.

Figures 7 and 8, 9 and 10 are the corresponding results for tracking error comparison and voltage comparison when the input signals are combined with certain measurement noise, respectively. We denote the input signals of X and Y axis as X_{original} and Y_{original}, $X_{\text{original}}, Y_{\text{original}} \in R^N$. Considering the noise signals to X and Y axis as ε_X and ε_Y, in which satisfy Gauss distribution:

$$\varepsilon_X \sim N(0, 0.002\% \left\|X_{\text{original}}\right\|_\infty), \quad \varepsilon_Y \sim N(0, 0.002\% \left\|Y_{\text{original}}\right\|_\infty).$$

Hence, the real input signals are:

$$X_{\text{real}} = X_{\text{original}} + \varepsilon_X, \quad Y_{\text{real}} = Y_{\text{original}} + \varepsilon_Y.$$

The simulation shows that the designed controllers have certain filtering effect for measurement noise. Obviously, ESO is superior to the RESO in filtering effect for its higher order.

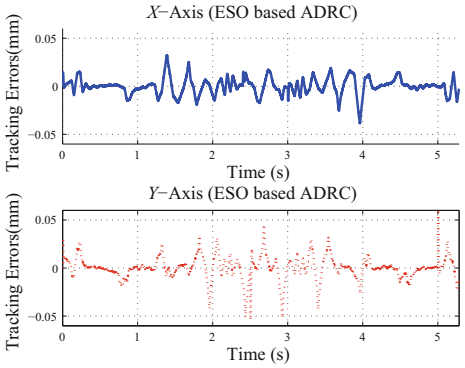

Figure 7 Tracking error of ESO-ADRC with measurement noise

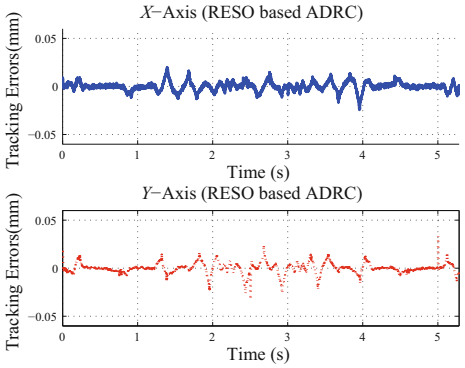

Figure 8 Tracking error of RESO-ADRC with measurement noise

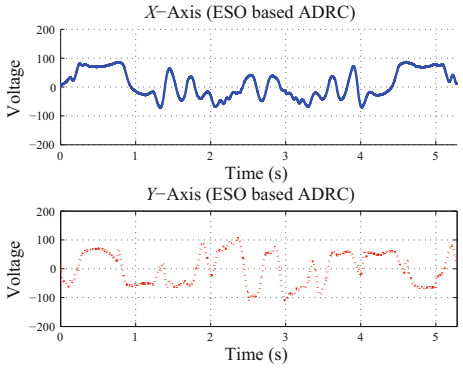

Figure 9 Voltage of ESO-ADRC with measurement noise

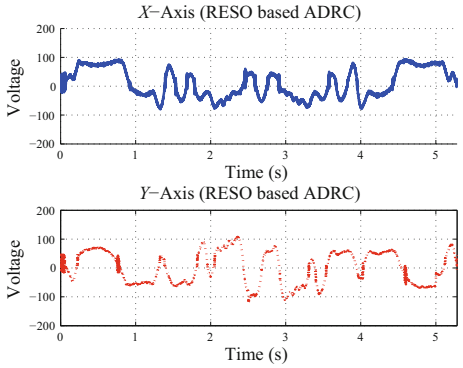

Figure 10 Voltage of RESO-ADRC with measurement noise

Remark 5.1 RESO performs better than the ESO both in disturbance estimation and tracking error. The physical reason for this phenomenon should be addressed more vividly. Actually, for ESO, $\widehat{x}_3 = \frac{\omega_e^3}{(s+\omega_e)^3}x_3$; for RESO $\widehat{x}_3 = \frac{\omega_e^2}{(s+\omega_e)^2}x_3$. Thus, RESO performs better than ESO both in estimation speed toward the disturbance and compensation speed toward the disturbance, and hence the closed-loop property is better. On the other hand, the above transfer functions mean that ESO is superior to the RESO in filtering the measurement noise. Hence, we suggest to choose the ESO based ADRC and RESO based ADRC according to the specific properties of the plant.

6 Conclusion

The permanent magnet linear motor (PMLM) has high speed, high precision, and is widely used in CNC machining. However, because of its nonlinearity and uncertainty as well as easily being subjected to the existing outside disturbance, the traditional control method such as PID is hard to meet its performance requirements. To improve the performance of the system PMLM, this paper utilizes the ADRC to design the controller in the system of PMLM due to its good performance, robust, and simple for implementing.

To mimic the practical manufacture situation, the nonlinear load force of PMLM, including friction and magnetic resistance as well as the nonlinear disturbances are considered. The stability of closed-loop system is proved. The control accuracy and quality are analyzed. We use a tangible manufacture example from CNC machining to perform the simulation of PMLM. ADRCs using ESO and RESO are implemented to specify the effects of these two methods respectively.

The result showed the effectiveness and feasibility of both ESO and RESO. Moreover, compared with ESO, RESO exhibits better performance at the cost of a little vibration in control signal.

References

[1] Brandenburg G, Bruckl S, Dormann J, et al., Comparative investigation of rotary and linear motor feed drive systems for high precision machine tools, *International Workshop on Advanced Motion Control*, 2000, 384–389.

[2] Seamus G and Michael T H, Development of a high-speed CNC cutting machine using linear motors, *Journal of Materials Processing Technology*, 2005, **166**(3): 321–329.

[3] Lin F J, Shyu K K, and Lin C H, Incremental motion control of linear synchronous motor, *IEEE Transactions on Aerospace and Electronic Systems*, 2002, **38**(3): 1011–1022.

[4] Chong G and Li Y, PID control system analysis, design, and technology, *IEEE Transactions Conontrol Systems Technology*, 2005, **13**(4): 559–576.

[5] Narendra and Kumpati S, Robust adaptive control, *American Control Conference*, 1984.

[6] Bristow D, Tharayil M, and Alleyne A G, A survey of iterative learning control, *IEEE Conontrol Systems Magazine*, 2006, **26**(3): 96–114.

[7] Guo B and Zhao Z, On convergence of the nonlinear active disturbance rejection control for mimo systems, *SIAM J. Control and Optimization*, 2013, **51**(2): 1727–1757.

[8] Zheng Q, Chen Z Z, and Gao Z Q, A practical approach to disturbance decoupling control, *Control Engineering Practice*, 2009, **17**(9): 1016–1025.

[9] Xue W C and Huang Y, On performance analysis of ADRC for nonlinear uncertain systems with unknown dynamics and discontinuous disturbances, 2013 *Chinese Control Conference*, 2013, 1102–1107.

[10] Dong J Y and Li D H, Active disturbance rejection control for complex dynamical systems, *System Science and Mathematic*, 2013, **33**(6): 639–652 (in Chinese).

[11] Jiang Z, Active disturbance rejection control for the yaw tracking for helicopter, *System Science and Mathematic*, 2012, **32**(6): 641—652 (in Chinese).

[12] Zheng Q, Gao L Q, and Gao Z, On validation of extended state observer through analysis and experimentation, *Journal of Dynamic Systems Measurement & Control*, 2012, **134**(2): 224–240.

[13] Xiao Y and Zhu K Y, Optimal synchronization control of highprecision motion systems, *IEEE Transactions on Industrial Electronics*, 2006, **53**(4): 1160–1169.

[14] Canudas-De-Wit C, Olsson H, Astrom K J, et al., A new model for control of systems with friction, *IEEE Transactions on Automatic Control*, 1995, **40**(3): 419–425.

[15] Tan K K, Huang S N, and Lee T H, Robust adaptive numerical compensation for friction and

force ripple in permanent-magnet linear motors, *IEEE Transactions on Magnetics*, 2002, **38**(1): 221–228.

[16] Han J Q, Auto-disturbances-rejection controller and its application, *Control and Decision*, 1998, **13**(1): 19–23.

[17] Gao Z Q, Haung Y, and Han J Q, An alternative paradigm for control system design, *IEEE Conference on Decision and Control*, 2001, **5**: 4578–4585.

[18] Xue W C, Theoretical analysis of active disturbance rejection control, Ph.D. Thesis, 2012.

[19] Hu T, Xue W C, and Huang Y, Active disturbance rejection control for permanent magnet linear motor, *Proceedings of the* 31*st Chinese Control Conference*, 2012, 296–301.

[20] Castelino K, D'Souza R, and Wright P K, Tool path optimization for minimizing airtime during machining, *Journal of Manufacturing Systems*, 2003, **22**(3): 173–180.

[21] Guo J X, Zhang Q, Gao X S, et al., Time optimal feedrate generation with confined tracking error based on linear programming, *Journal of Systems Science and Complexity*, 2015, **28**(1): 80–95.

[22] Zhang K, Gao X S, Li H, and Yuan C M, A greedy algorithm for feed-rate planning of CNC machines along curved tool paths with confined jerk for each axis, *Robotics and computer Integrated Manufacturing*, 2012, **28**: 472–483.

[23] Fan W, Gao X S, Yan W, et al., Interpolation of parametric CNC machining path under confined jounce, *The International Journal of Advanced Manufacturing Technology*, 2012, **62**(5–8): 719–739.

[24] Zhao C and Huang Y, ADRC bsed input disturbance rejection for minimum-phase plants with unknown orders and/or uncertain relative degrees, *Journal of Systems Science and Complexity*, 2012, **25**(4): 625–640.

[25] Yau H T, Lin M T, and Tsai M S, Real-time NURBS interpolation using FPGA for high speed motion control, *Computer-Aided Design*, 2006, **38**: 1123–1133.

[26] Erkorkmaz K and Altintas Y, High speed CNC system design Part I: Jerk limited trajectory generation and quintic spline interpolation, *International Journal of Machine Tools and Manufacture*, 2001, **41**: 1323–1345.

[27] Altintas Y and Erkorkmaz K, Feedrate optimization for spline interpolation in high speed machine tools, *CIRP Annals—Manufacturing Technology*, 2003, **52**(1): 297–302.

Appendix

Before giving the corresponding proof, the closed-loop form of ESO and RESO are rendered respectively.

From(1), (4), (5), (10), (73), we get the closed-loop system of ESO:

$$\begin{pmatrix} \dot{\widetilde{x}}_1 \\ \dot{\widetilde{x}}_2 \\ \dot{\zeta}_1 \\ \dot{\zeta}_2 \\ \dot{\zeta}_3 \end{pmatrix} = \begin{pmatrix} 0 & 1 & 0 & 0 & 0 \\ -\omega_c^2 & -2\omega_c & -\omega_c^2/\omega^2 & -2\omega_c/\omega & -1 \\ 0 & 0 & -3\omega & \omega & 0 \\ 0 & 0 & -3\omega & 0 & \omega \\ 0 & 0 & -\omega & 0 & 0 \end{pmatrix} \begin{pmatrix} \widetilde{x}_1 \\ \widetilde{x}_2 \\ \zeta_1 \\ \zeta_2 \\ \zeta_3 \end{pmatrix} + \begin{pmatrix} 0 \\ -f_0 \\ 0 \\ \omega f_0 \\ \eta_3 \end{pmatrix}, \tag{16}$$

where

$$\zeta = \begin{pmatrix} \zeta_1 \\ \zeta_2 \\ \zeta_3 \end{pmatrix} = \begin{pmatrix} \omega^2 \overline{e}_1 \\ \omega \overline{e}_2 \\ \overline{e}_3 - f_0 \end{pmatrix}, \tag{17}$$

$\eta_3 = -(\omega_c^2 \widetilde{x}_1 + 2\omega_c \widetilde{x}_2 + \frac{\omega_c^2}{\omega^2}\zeta_1 + 2\frac{\omega_c}{\omega}\zeta_2 + \zeta_3 + f_0)\widetilde{a}_1 + (\omega_c^2 v + 2\omega_c \dot{v} + \ddot{v} - \omega_c^2 x_1^* - 2\omega_c x_2^*)\widetilde{a}_1$, $\widetilde{a}_1 = a_1 + f_v$.

Besides, from (5), (8), (10), (20), we can obtain the closed-loop system of RESO:

$$\begin{pmatrix} \dot{\widetilde{x}}_1 \\ \dot{\widetilde{x}}_2 \\ \dot{\xi}_2 \\ \dot{\xi}_3 \end{pmatrix} = \begin{pmatrix} 0 & 1 & 0 & 0 \\ -\omega_c^2 & -2\omega_c & -2\omega_c/\omega & -1 \\ 0 & 0 & -2\omega & \omega \\ 0 & 0 & -\omega & 0 \end{pmatrix} \begin{pmatrix} \widetilde{x}_1 \\ \widetilde{x}_2 \\ \xi_2 \\ \xi_3 \end{pmatrix} + \begin{pmatrix} 0 \\ -f_0 \\ \omega f_0 \\ \eta_1 \end{pmatrix}, \tag{18}$$

where

$$\xi = \begin{pmatrix} \xi_2 \\ \xi_3 \end{pmatrix} = \begin{pmatrix} \omega \widehat{e}_2 \\ \widehat{e}_3 - f_0 \end{pmatrix}. \tag{19}$$

and $\eta_1 = -(\omega_c^2 \widetilde{x}_1 + 2\omega_c \widetilde{x}_2 + \frac{2\omega_c}{\omega}\xi_2 + \xi_3 + f_0)\widetilde{a}_1 + (\omega_c^2 v + 2\omega_c \dot{v} + \ddot{v} - \omega_c^2 x_1^* - 2\omega_c x_2^*)\widetilde{a}_1$, $\widetilde{a}_1 = a_1 + f_v$.

The proof from ESO is similar to that from RESO. Nevertheless, the proof of RESO is more presentative, which helps to understand the principle and process of the proof. Hence, we give more detail to RESO initially.

Appendix A The Proof of Theorem 4.2

We will prove the theorem in two steps.

Step 1 Prove that x_1, x_2, $\widehat{e}_2$, $\widehat{e}_3$ are bounded in $[t_0, \infty)$.

Make transformation

$$\xi = \begin{pmatrix} \xi_2 \\ \xi_3 \end{pmatrix} = \begin{pmatrix} \omega \widehat{e}_2 \\ \widehat{e}_3 - f_0 \end{pmatrix}. \tag{20}$$

Define

$$A_c = \begin{pmatrix} 0 & 1 \\ -\omega_c^2 & -2\omega_c \end{pmatrix}, \quad B_c = \begin{pmatrix} 0 & 0 \\ -2\omega_c/\omega & -1 \end{pmatrix}, \quad A_2 = \begin{pmatrix} -2 & 1 \\ -1 & 0 \end{pmatrix}.$$

Since A_c, A_2 are Hurwitz matrixes, there exist positive matrixes $P_1 = \begin{pmatrix} m & n \\ n & l \end{pmatrix}$ and $P_2 = \begin{pmatrix} p & q \\ q & r \end{pmatrix}$, satisfying

$$A_c^{\mathrm{T}} P_1 + P_1 A_c = -I_2, \quad c_{11} I_2 \le P_1 \le c_{12} I_2, \tag{21}$$

$$A_2^{\mathrm{T}} P_2 + P_2 A_2 = -I_2, \quad c_{21} I_2 \le P_2 \le c_{22} I_2, \tag{22}$$

where c_{11}, c_{12} are the minimum and maximum eigenvalues of P_1; c_{21}, c_{22} are the minimum and maximum eigenvalues of P_2. From (21), (22), we have

$$\begin{aligned}
&P_1 = \begin{pmatrix} \frac{\omega_c^2+5}{4\omega_c} & \frac{1}{2\omega_c^2} \\ \frac{1}{2\omega_c^2} & \frac{\omega_c^2+1}{4\omega_c^3} \end{pmatrix},\ P_2 = \begin{pmatrix} \frac{1}{2} & -\frac{1}{2} \\ -\frac{1}{2} & \frac{3}{2} \end{pmatrix}, \\
&c_{11} = \frac{1}{8\omega_c^3}\left[\omega_c^4 + 6\omega_c^2 + 1 - \sqrt{(\omega_c^4 + 6\omega_c^2 + 1)(\omega_c^4 + 2\omega_c^2 + 1)}\right], \\
&c_{12} = \frac{1}{8\omega_c^3}\left[\omega_c^4 + 6\omega_c^2 + 1 + \sqrt{(\omega_c^4 + 6\omega_c^2 + 1)(\omega_c^4 + 2\omega_c^2 + 1)}\right], \\
&c_{21} = \frac{2-\sqrt{2}}{2}, \quad c_{22} = \frac{2+\sqrt{2}}{2}.
\end{aligned} \tag{23}$$

$\|\cdot\|$ below is the 2-norm. Define Lyapunov function, along the trajectory of (18): $V_1(\widetilde{x}) = \widetilde{x}^{\mathrm{T}} P_1 \widetilde{x}$

$$\begin{aligned}
\dot{V}_1(\widetilde{x}) = 2\widetilde{x}^{\mathrm{T}} P_1 \dot{\widetilde{x}} &= -\|\widetilde{x}\|^2 + 2\widetilde{x}^{\mathrm{T}} P_1 (B_c \xi + (\,0\ 1\,)^{\mathrm{T}}(-f_0)) \\
&\le -\|\widetilde{x}\|^2 + 2\|\widetilde{x}\| \cdot \|P_1 B_c\| \cdot \|\xi\| + 2\|\widetilde{x}\| \cdot \|P_1 (\,0\ 1\,)^{\mathrm{T}} f_0\|.
\end{aligned}$$

In the formula above, when $\omega \ge 2\omega_c$, the second and the last parts of the equation are

$$\begin{aligned}
\|P_1 B_c\| \le \sqrt{2}\|P_1 B_c\|_1 &= \sqrt{2}\left\| \begin{pmatrix} -2n\omega_c/\omega & -n \\ -2l\omega_c/\omega & -l \end{pmatrix} \right\|_1 \\
&= \sqrt{2}(n+l)\max\{2\omega_c/\omega, 1\} \\
&= \sqrt{2}\left(\frac{1}{2\omega_c^2} + \frac{\omega_c^2+1}{4\omega_c^3}\right), \\
\|P_1\big(\,0\ 1\,\big)^{\mathrm{T}} f_0\| = |f_0|\sqrt{n^2+l^2} &= |f_0|\sqrt{\left(\frac{1}{2\omega_c^2}\right)^2 + \left(\frac{\omega_c^2+1}{4\omega_c^3}\right)^2}.
\end{aligned}$$

Due to the bound of the $|f_0|$ ($f_0 = \frac{1}{M}(F_{\mathrm{load}} + F_{\mathrm{ripple}})$), suppose $|f_0| \le \kappa_1$ and define

$$r_1(\omega_c) = 2\sqrt{2}\left(\frac{1}{2\omega_c^2} + \frac{\omega_c^2+1}{4\omega_c^3}\right), \tag{24}$$

$$r_2(\omega_c) = 2\sqrt{\left(\frac{1}{2\omega_c^2}\right)^2 + \left(\frac{\omega_c^2+1}{4\omega_c^3}\right)^2}. \tag{25}$$

Then

$$\dot{V}_1(\widetilde{x}) \le -\|\widetilde{x}\|^2 + r_1(\omega_c)\|\widetilde{x}\| \cdot \|\xi\| + \kappa_1 r_2(\omega_c)\|\widetilde{x}\|. \tag{26}$$

Construct Lyapunov function: $V_2(\xi) = \xi^{\mathrm{T}} P_2 \xi$ and define $K_1 = (\,\omega_c^2\ 2\omega_c\,)$, $K_2 = (\,2\omega_c/\omega\ 1\,)$, $R = (\,\omega f_0\ \eta_1\,)^{\mathrm{T}}$.

Along the trajectory of (18):

$$\begin{aligned}
\dot{V}_2(\xi) &= 2\xi^{\mathrm{T}} P_2(\omega A_2 \xi + R) \\
&= -\omega\|\xi\|^2 + 2\omega\xi^{\mathrm{T}} P_2(\,1\ 0\,)^{\mathrm{T}} f_0 + 2\xi^{\mathrm{T}} P_2(\,0\ 1\,)^{\mathrm{T}}(-K_1\widetilde{x} - K_2\xi - f_0 \\
&\quad + \omega_c^2 v + 2\omega_c\dot{v} + \ddot{v} - \omega_c^2 x_1^* - 2\omega_c x_2^*)\widetilde{a}_1.
\end{aligned}$$

Suppose $|f_0-(\omega_c^2 v+2\omega_c\dot{v}+\ddot{v}-\omega_c^2 x_1^*-2\omega_c x_2^*)|\le\kappa_2$, and define

$$s_1(\omega_c)=|\widetilde{a}_1|\sqrt{10((2\omega_c)^2+\omega_c^4)}, \tag{27}$$

$$s_2=2\sqrt{5}|\widetilde{a}_1|, \tag{28}$$

$$s_3=\kappa_2\sqrt{10}|\widetilde{a}_1|. \tag{29}$$

Hence, when $\omega\ge 2\omega_c$, in consideration of

$$\|P_2\begin{pmatrix}0&1\end{pmatrix}^{\mathrm{T}}K_1\|\le\left\|\begin{pmatrix}\frac{1}{2}&-\frac{1}{2}\\-\frac{1}{2}&\frac{3}{2}\end{pmatrix}\begin{pmatrix}0&1\end{pmatrix}^{\mathrm{T}}\right\|\cdot\|\begin{pmatrix}\omega_c^2&2\omega_c\end{pmatrix}\|=\frac{s_1(\omega_c)}{2|\widetilde{a}_1|},$$

$$\|P_2\begin{pmatrix}0&1\end{pmatrix}^{\mathrm{T}}K_2\|\le\left\|\begin{pmatrix}\frac{1}{2}&-\frac{1}{2}\\-\frac{1}{2}&\frac{3}{2}\end{pmatrix}\begin{pmatrix}0&1\end{pmatrix}^{\mathrm{T}}\right\|\cdot\|\begin{pmatrix}2\omega_c/\omega&1\end{pmatrix}\|\le\frac{s_2}{2|\widetilde{a}_1|},$$

$$\|P_2\begin{pmatrix}0&1\end{pmatrix}^{\mathrm{T}}(f_0-(\omega_c^2 v+2\omega_c\dot{v}+\ddot{v}-\omega_c^2 x_1^*-2\omega_c x_2^*))\|\le\frac{s_3}{2|\widetilde{a}_1|},$$

we have

$$\dot{V}_2(\xi)\le-(\omega-s_2)\|\xi\|^2+(\sqrt{2}\omega\kappa_1+s_3)\|\xi\|+s_1(\omega_c)\|\widetilde{x}\|\cdot\|\xi\|. \tag{30}$$

Define

$$\rho_1=\max\left\{\sqrt{V_1(\widetilde{x}(t_0))},\ 2\sqrt{c_{12}}\left[\frac{\rho_2}{\sqrt{c_{21}}}r_1(\omega_c)+\kappa_1 r_2(\omega_c)\right]\right\}, \tag{31}$$

$$\rho_2=\max\{\sqrt{V_2(\xi(t_0))},\ (\sqrt{2}+1)\sqrt{c_{22}}\kappa_1\}. \tag{32}$$

We will prove that when $\omega>\frac{1}{\kappa_1}(\frac{\rho_2}{\sqrt{c_{22}}}s_1(\omega_c)\frac{\rho_1}{\sqrt{c_{11}}}+s_2+s_3)$, then $\Omega=\{(\widetilde{x}(t_0),\xi)|\sqrt{V_1(\widetilde{x})}\le\rho_1,\ \sqrt{V_2(\xi)}\le\rho_2\}$ is a positive invariant set of (18). We develop the proof in two situations:

i) if $\sqrt{V_1(\widetilde{x})}=\rho_1$, $\sqrt{V_2(\xi)}\le\rho_2$, then from (26), along the trajectory of (18), we have

$$\begin{aligned}\dot{V}_1(\widetilde{x})&\le-\|\widetilde{x}\|\cdot[\|\widetilde{x}\|-(r_1(\omega_c)\|\xi\|+\kappa_1 r_2(\omega_c))]\\&\le-\|\widetilde{x}\|\cdot\left[\frac{\rho_1}{\sqrt{c_{12}}}-\left(r_1(\omega_c)\frac{\rho_2}{\sqrt{c_{21}}}+\kappa_1 r_2(\omega_c)\right)\right]\\&\le-\|\widetilde{x}\|\cdot\left[r_1(\omega_c)\frac{\rho_2}{\sqrt{c_{21}}}+\kappa_1 r_2(\omega_c)\right]\\&\le 0;\end{aligned} \tag{33}$$

ii) if $\sqrt{V_1(\widetilde{x})}\le\rho_1$, $\sqrt{V_2(\xi)}=\rho_2$, then from (30), along the trajectory of (18), we have

$$\begin{aligned}\dot{V}_2(\xi)&\le-\|\xi\|\cdot[(\omega-s_2)\|\xi\|-((\sqrt{2}\omega\kappa_1+s_3)+s_1(\omega_c)\|\widetilde{x}\|)]\\&\le-\|\xi\|\cdot\left[(\omega-s_2)\frac{\rho_2}{\sqrt{c_{22}}}-\left((\sqrt{2}\omega\kappa_1+s_3)+s_1(\omega_c)\frac{\rho_1}{\sqrt{c_{11}}}\right)\right]\\&\le-\|\xi\|\cdot\left[\left(\frac{\rho_2}{\sqrt{c_{22}}}-\sqrt{2}\kappa_1\right)\omega-\left(\frac{\rho_2}{\sqrt{c_{22}}}s_2+s_3+s_1(\omega_c)\frac{\rho_1}{\sqrt{c_{11}}}\right)\right]\\&\le-\|\xi\|\cdot\left[\kappa_1\omega-\left(\frac{\rho_2}{\sqrt{c_{22}}}s_2+s_3+s_1(\omega_c)\frac{\rho_1}{\sqrt{c_{11}}}\right)\right]\\&<0.\end{aligned} \tag{34}$$

From (33) and (34), we can come to the comclusion: If $\omega > \frac{1}{\kappa_1}(\frac{\rho_1}{\sqrt{c_{11}}}s_1(\omega_c) + \frac{\rho_2}{\sqrt{c_{22}}}s_2 + s_3)$, Ω is a positive invariant set of (18).

From the analysis above, we can draw the conclusion that when the bandwidth of RESO ω and the bandwidth of control ω_c satisfy

$$\omega > \max\left\{2\omega_c,\ \frac{1}{\kappa_1}\left(\frac{\rho_1}{\sqrt{c_{11}}}s_1(\omega_c) + \frac{\rho_2}{\sqrt{c_{22}}}s_2 + s_3\right)\right\}, \tag{35}$$

then $\|\widetilde{x}\|$, $\|\xi\|$ are bounded:

$$\|\widetilde{x}\| \leq \frac{\rho_1}{\sqrt{c_{11}}}, \quad \|\xi\| \leq \frac{\rho_2}{\sqrt{c_{21}}}. \tag{36}$$

Since $\widetilde{x} = \begin{pmatrix} x_1 - x^* \\ x_2 - \dot{x}^* \end{pmatrix}$, and x^*, $\dot{x}^*$are bounded, x_1 and x_2 are bounded. At the same time, from the transformation (20) we can get $\widehat{e}_2$, $\widehat{e}_3$ are bounded.

Step 2 Due to Assumption 1, the load force $|F_{\text{load}}(t)|$ only contains the first discontinuous points $\{t_i\}_{i=1}^{\infty}$, $t_{i-1} < t_i$, and $\inf_i\{t_i - t_{i-1}\} > 0$. Since $f_0 = \frac{1}{M}(F_{\text{load}} + F_{\text{ripple}})$, f_0 onle contains the discontinuous points of the first kind $\{t_i\}_{i=1}^{\infty}$, $t_{i-1} < t_i$, and $\inf_i\{t_i - t_{i-1}\} > 0$. Define $\delta_t = \inf_i\{t_i - t_{i-1}\}$. The derivative of f_0 in a general form can be defined as

$$\dot{f}_0 = \begin{cases} \dfrac{df_0}{dt}, & t \neq t_i, \\ H_i\delta(t - t_i), & t = t_i, \end{cases} \tag{37}$$

where $|\dot{f}_0| \leq D < \infty$, $|H_i| \leq H < \infty$, $\delta(\cdot)$ have the properties:

$$\int \delta(t - t_i)dt = \begin{cases} 0, & t < t_i \\ 1, & t \geq t_i. \end{cases}$$

Make a transformation:

$$\overline{\xi} = \begin{pmatrix} \overline{\xi}_2 \\ \overline{\xi}_3 \end{pmatrix} = \begin{pmatrix} \omega\widehat{e}_2 \\ \widehat{e}_3. \end{pmatrix}. \tag{38}$$

From (5), (8) and (10), we obtain the closed-loop

$$\begin{pmatrix} \dot{\widetilde{x}}_1 \\ \dot{\widetilde{x}}_2 \\ \dot{\overline{\xi}}_2 \\ \dot{\overline{\xi}}_3 \end{pmatrix} = \begin{pmatrix} 0 & 1 & 0 & 0 \\ -\omega_c^2 & -2\omega_c & -2\omega_c/\omega & -1 \\ 0 & 0 & -2\omega & \omega \\ 0 & 0 & -\omega & 0 \end{pmatrix} \begin{pmatrix} \widetilde{x}_1 \\ \widetilde{x}_2 \\ \overline{\xi}_2 \\ \overline{\xi}_3 \end{pmatrix} + \begin{pmatrix} 0 \\ 0 \\ 0 \\ \eta_2 \end{pmatrix}, \tag{39}$$

where

$$\eta_2 = -(\omega_c^2\widetilde{x}_1 + 2\omega_c\widetilde{x}_2 + 2\omega_c\widehat{e}_2 + \widehat{e}_3)\widetilde{a}_1 + (\omega_c^2 v + 2\omega_c\dot{v} + \ddot{v} - \omega_c^2 x_1^* - 2\omega_c x_2^*)\widetilde{a}_1 + \dot{f}_0. \tag{40}$$

Comparing (20) and (38), we can get

$$\begin{aligned}\|\overline{\xi}\| = \sqrt{\overline{\xi}_2^2 + \overline{\xi}_3^2} &= \sqrt{\xi_2^2 + (\xi_3 + f_0)^2} \\ &\le \sqrt{2} \cdot \sqrt{\xi_2^2 + \xi_3^2 + f_0^2} \\ &\le \sqrt{2}(\|\xi\| + |f_0|).\end{aligned}$$

Since ξ and f_0 are bounded, and $\|\xi\| \le \frac{\rho_2}{\sqrt{c_{21}}}$, $|f_0| \le \kappa_1$,

$$\|\overline{\xi}\| \le \rho_3, \quad \rho_3 = \sqrt{2}\Big(\frac{\rho_2}{\sqrt{c_{21}}} + \kappa_1\Big). \tag{41}$$

When $t_0 \le t < t_1$, along the trajectory (39),

$$\dot{V}_2(\overline{\xi}) = 2\overline{\xi}^{\mathrm{T}} P_2\big(\omega A_2 \overline{\xi} + \big(\begin{array}{cc}0 & 1\end{array}\big)^{\mathrm{T}} \eta_2\big).$$

Define $\|\eta_2(t)\| \le \kappa_3, t \ne t_i, i = 1, 2, \cdots$, here $\kappa_3 = \kappa_3(\omega_c, \rho_1, \rho_2, v, \dot{v}, \ddot{v}, A_r, D)$. Since η_2 is bounded in the continuous points of f_0, then

$$\|P_2(\begin{array}{cc}0 & 1\end{array})^{\mathrm{T}}\| \cdot |\eta_2| = \frac{\sqrt{10}}{2}|\eta_2| \le \frac{\sqrt{10}}{2}\kappa_3 = \frac{s_4}{2}, \tag{42}$$

where $s_4 = \sqrt{10}\kappa_3$.

Hence $\dot{V}_2(\overline{\xi}) \le -\omega\|\overline{\xi}\|^2 + s_4\|\overline{\xi}\|$, and

$$\begin{aligned}\frac{d}{dt}\sqrt{V_2(\overline{\xi})} = \frac{\dot{V}_2(\overline{\xi})}{2\sqrt{V_2(\overline{\xi})}} &\le -\omega\frac{\|\overline{\xi}\|^2}{2\sqrt{V_2(\overline{\xi})}} + \frac{s_4\|\overline{\xi}\|}{2\sqrt{V_2(\overline{\xi})}} \\ &\le -\omega\frac{\sqrt{V_2(\overline{\xi})}}{2c_{22}} + \frac{s_4}{2\sqrt{c_{21}}}.\end{aligned} \tag{43}$$

From Gronwall-Bellman inequation, we can get, when $t_0 \le t < t_1$,

$$\begin{aligned}\sqrt{V_2(\overline{\xi})} &\le \frac{1}{\omega}\frac{c_{22}s_4}{\sqrt{c_{21}}} + \sqrt{V_2(\overline{\xi}(t_0))}\mathrm{e}^{-\frac{\omega}{2c_{22}}(t-t_0)} \\ &\le \frac{1}{\omega}\frac{c_{22}s_4}{\sqrt{c_{21}}} + \sqrt{c_{22}}\|\overline{\xi}(t_0)\|\mathrm{e}^{-\frac{\omega}{2c_{22}}(t-t_0)} \\ &\le \frac{1}{\omega}\frac{c_{22}s_4}{\sqrt{c_{21}}} + \rho_3\sqrt{c_{22}}\mathrm{e}^{-\frac{\omega}{2c_{22}}(t-t_0)}.\end{aligned} \tag{44}$$

If $\delta_t = \inf_i\{t_i - t_{i-1}\} \le \frac{2c_{22}}{e}$, then $\{\omega|\delta_t = \frac{2c_{22}\ln\omega}{\omega}\} \ne \emptyset$. Define

$$\omega_1 = \begin{cases}\max\Big\{\omega|\delta_t = \dfrac{2c_{22}\ln\omega}{\omega}\Big\}, & \delta_t \le \dfrac{2c_{22}}{e}, \\ 0, & \delta_t > \dfrac{2c_{22}}{e}.\end{cases} \tag{45}$$

Then when $\omega > \omega_1$, we have

$$\frac{2c_{22}\ln\omega}{\omega} < \delta_t. \tag{46}$$

Define

$$t_0^* = t_0 + \frac{2c_{22}\ln\omega}{\omega}. \tag{47}$$

From (45), $t_0^* < t_1$, then

$$\mathrm{e}^{-\frac{\omega}{2c_{22}}(t-t_0)} \le \frac{1}{\omega}, \quad t \ge t_0^*. \tag{48}$$

From (44) and (48), we get

$$\sqrt{V_2(\overline{\xi})} \le \frac{1}{\omega}\left(\frac{c_{22}s_4}{\sqrt{c_{21}}} + \rho_3\sqrt{c_{22}}\right), \quad t \in [t_0^*, t_1). \tag{49}$$

Hence,

$$\|\overline{\xi}\| \le \frac{1}{\omega}\left(\frac{c_{22}}{c_{21}}s_4 + \frac{\sqrt{c_{22}}}{\sqrt{c_{21}}}\rho_3\right), \quad t \in [t_0^*, t_1). \tag{50}$$

From the transformation (38), we get

$$\|\widehat{e}\| \le \|\overline{\xi}\| \le \frac{1}{\omega}\left(\frac{c_{22}}{c_{21}}s_4 + \frac{\sqrt{c_{22}}}{\sqrt{c_{21}}}\rho_3\right), \quad t \in [t_0^*, t_1). \tag{51}$$

Similar to (44), when $t_1 \le t < t_2$,

$$\begin{aligned}\sqrt{V_2(\overline{\xi})} &\le \frac{1}{\omega}\frac{c_{22}s_4}{\sqrt{c_{21}}} + \sqrt{V_2(\overline{\xi}(t_1^+))}\mathrm{e}^{-\frac{\omega}{2c_{22}}(t-t_1)} \\ &\le \frac{1}{\omega}\frac{c_{22}s_4}{\sqrt{c_{21}}} + \sqrt{c_{22}}\|\xi(t_1^+)\|\mathrm{e}^{-\frac{\omega}{2c_{22}}(t-t_1)} \\ &\le \frac{1}{\omega}\frac{c_{22}s_4}{\sqrt{c_{21}}} + \rho_3\sqrt{c_{22}}\mathrm{e}^{-\frac{\omega}{2c_{22}}(t-t_1)}.\end{aligned} \tag{52}$$

Define

$$t_1^* = t_1 + \frac{2c_{22}\ln\omega}{\omega}. \tag{53}$$

Then

$$\mathrm{e}^{-\frac{\omega}{2c_{22}}(t-t_1)} \le \frac{1}{\omega}, \quad t \ge t_1^*. \tag{54}$$

From (52) and (54), we obtain

$$\sqrt{V_2(\overline{\xi})} \le \frac{1}{\omega}\left(\frac{c_{22}s_4}{\sqrt{c_{21}}} + \rho_3\sqrt{c_{22}}\right), \quad t \in [t_1^*, t_2). \tag{55}$$

Hence,

$$\|\overline{\xi}\| \le \frac{1}{\omega}\left(\frac{c_{22}}{c_{21}}s_4 + \frac{\sqrt{c_{22}}}{\sqrt{c_{21}}}\rho_3\right), \quad t \in [t_1^*, t_2). \tag{56}$$

Similarly, we can prove for $i \geq 0$,

$$\|\overline{\xi}\| \leq \frac{1}{\omega}\left(\frac{c_{22}}{c_{21}}s_4 + \frac{\sqrt{c_{22}}}{\sqrt{c_{21}}}\rho_3\right), \quad t \in [t_i^*, t_{i+1}), \tag{57}$$

where

$$t_i^* = t_i + \frac{2c_{22}\ln\omega}{\omega}. \tag{58}$$

From the transformation (38), for $i \geq 1$,

$$\|\widehat{e}\| \leq \|\overline{\xi}\| \leq \frac{1}{\omega}\left(\frac{c_{22}}{c_{21}}s_4 + \frac{\sqrt{c_{22}}}{\sqrt{c_{21}}}\rho_3\right), \quad t \in [t_i^*, t_{i+1}). \tag{59}$$

Next, we will prove that, when ω is large enough ($\omega \gg 1$), $\|x(t) - x^*(t)\| \leq O(\frac{\ln\omega}{\omega})$, $t \in [t_0, \infty)$.

Along the trajectory of (39) we have

$$\dot{V}_1(\widetilde{x}) = 2\widetilde{x}^{\mathrm{T}}P_1\dot{\widetilde{x}} \leq -\|\widetilde{x}\|^2 + r_1(\omega_c)\|\overline{\xi}\| \cdot \|\widetilde{x}\|.$$

So

$$\begin{aligned}\frac{d}{dt}\sqrt{V_1(\widetilde{x})} = \frac{\dot{V}_1(\widetilde{x})}{2\sqrt{V_1(\widetilde{x})}} &\leq -\frac{\|\widetilde{x}\|^2}{2\sqrt{V_1(\widetilde{x})}} + \frac{r_1(\omega_c)\|\widetilde{x}\| \cdot \|\overline{\xi}\|}{2\sqrt{V_1(\widetilde{x})}} \\ &\leq -\frac{\sqrt{V_1(\widetilde{x})}}{2c_{12}} + \frac{r_1(\omega_c)}{2\sqrt{c_{11}}}\|\overline{\xi}\|.\end{aligned}$$

Since $\widetilde{x}(t_0) = 0$, from Gronwall-Bellman inequation, we get

$$\sqrt{V_1(\widetilde{x})} \leq \frac{r_1(\omega_c)}{2\sqrt{c_{11}}}\int_{t_0}^{t} \mathrm{e}^{-\frac{t-\tau}{2c_{12}}}\|\overline{\xi}(\tau)\|d\tau. \tag{60}$$

When $t_{k-1} \leq t < t_k$,

$$\begin{aligned}\sqrt{V_1(\widetilde{x})} \leq \frac{r_1(\omega_c)}{2\sqrt{c_{11}}}\Bigg(&\sum_{i=1}^{k}\int_{t_{i-1}}^{t_{i-1}^*} \mathrm{e}^{-\frac{t-\tau}{2c_{12}}}\|\overline{\xi}(\tau)\|d\tau + \sum_{i=1}^{k-1}\int_{t_{i-1}^*}^{t_i} \mathrm{e}^{-\frac{t-\tau}{2c_{12}}}\|\overline{\xi}(\tau)\|d\tau \\ &+ \int_{t_{k-1}^*}^{t} \mathrm{e}^{-\frac{t-\tau}{2c_{12}}}\|\overline{\xi}(\tau)\|d\tau\Bigg).\end{aligned} \tag{61}$$

From (41),

$$\sum_{i=1}^{k-1}\int_{t_{i-1}^*}^{t_i} \mathrm{e}^{-\frac{t-\tau}{2c_{12}}}\|\overline{\xi}(\tau)\|d\tau + \int_{t_{k-1}^*}^{t} \mathrm{e}^{-\frac{t-\tau}{2c_{12}}}\|\overline{\xi}(\tau)\|d\tau < \left(\frac{c_{22}}{c_{21}}s_4 + \frac{\sqrt{c_{22}}}{\sqrt{c_{21}}}H\right)\frac{1}{\omega}, \tag{62}$$

$$\sum_{i=1}^{k}\int_{t_{i-1}}^{t_{i-1}^*} \mathrm{e}^{-\frac{t-\tau}{2c_{12}}}\|\overline{\xi}(\tau)\|d\tau \leq 4c_{22}\rho_3\frac{\ln\omega}{\omega}\sum_{i=1}^{k}\mathrm{e}^{-\frac{t-t_i}{2c_{12}}} \leq 4c_{22}\rho_3\frac{\mathrm{e}^{\frac{\delta_t}{2c_{12}}}}{1-\mathrm{e}^{-\frac{\delta_t}{2c_{12}}}}\frac{\ln\omega}{\omega}. \tag{63}$$

Then, from (61), (62) and (63), we get

$$\sqrt{V_1(\widetilde{x})} \leq \frac{r_1(\omega_c)}{2\sqrt{c_{11}}}\left[\left(\frac{c_{22}}{c_{21}}s_4 + \frac{\sqrt{c_{22}}}{\sqrt{c_{21}}}\rho_3\right)\frac{1}{\omega} + 4c_{22}\rho_3\frac{\mathrm{e}^{\frac{\delta_t}{2c_{12}}}}{1-\mathrm{e}^{-\frac{\delta_t}{2c_{12}}}}\frac{\ln\omega}{\omega}\right]. \tag{64}$$

Hence,

$$\|\widetilde{x}\| \leq \frac{r_1(\omega_c)}{2c_{11}}\left[\left(\frac{c_{22}}{c_{21}}s_4+\frac{\sqrt{c_{22}}}{\sqrt{c_{21}}}\rho_3\right)\frac{1}{\omega}+4c_{22}\rho_3\frac{\mathrm{e}^{\frac{\delta_t}{2c_{12}}}}{1-\mathrm{e}^{-\frac{\delta_t}{2c_{12}}}}\frac{\ln\omega}{\omega}\right]. \tag{65}$$

When $(\frac{c_{22}}{c_{21}}s_4+\frac{\sqrt{c_{22}}}{\sqrt{c_{21}}}H)\frac{1}{\omega}\leq 4c_{22}\rho_3\frac{\mathrm{e}^{\frac{\delta_t}{2c_{12}}}}{1-\mathrm{e}^{-\frac{\delta_t}{2c_{12}}}}\frac{\ln\omega}{\omega}$, namely,

$$\omega\geq\omega_2=\exp\left(\frac{\frac{c_{22}}{c_{21}}s_4+\frac{\sqrt{c_{22}}}{\sqrt{c_{21}}}H}{4c_{22}\rho_3}\cdot\frac{\mathrm{e}^{\frac{\delta_t}{2c_{12}}}-1}{\mathrm{e}^{\frac{\delta_t}{c_{12}}}}\right), \tag{66}$$

$$\|\widetilde{x}\|\leq\frac{4c_{22}\rho_3 r_1(\omega_c)}{c_{11}}\cdot\frac{\mathrm{e}^{\frac{\delta_t}{c_{12}}}}{\mathrm{e}^{\frac{\delta_t}{2c_{12}}}-1}\cdot\frac{\ln\omega}{\omega}. \tag{67}$$

To sum up, from (45), (51), (59), (66) and (67), when $\omega\geq\omega^*$ we have

$$\omega^*=\max\left\{2\omega_c,\ \frac{1}{\kappa_1}\left(\frac{\rho_1}{\sqrt{c_{11}}}s_1(\omega_c)+\frac{\rho_2}{\sqrt{c_{22}}}s_2+s_3\right),\omega_1,\omega_2\right\}, \tag{68}$$

$$\|\widehat{e}(t)\|\leq T_1\cdot\frac{1}{\omega},\quad t\in\left[t_{i-1}+2c_{22}\frac{\ln\omega}{\omega},t_i\right), \tag{69}$$

$$\|\widetilde{x}\|\leq T_2\cdot\frac{\ln\omega}{\omega},\quad t\in[t_0,\infty), \tag{70}$$

where

$$T_1=\frac{c_{22}}{c_{21}}s_4+\frac{\sqrt{c_{22}}}{\sqrt{c_{21}}}\rho_3, \tag{71}$$

$$T_2=\frac{4c_{22}\rho_3 r_1(\omega_c)}{c_{11}}\cdot\frac{\mathrm{e}^{\frac{\delta_t}{c_{12}}}}{\mathrm{e}^{\frac{\delta_t}{2c_{12}}}-1}, \tag{72}$$

are constants depend on ω_c, the initial values, the uncertainty and the reference signals.

Appendix B The Proof of Theorem 4.1

The proof is similar to that of Theorem 4.2. We only render the important variables form so that can make comparison with RESO.

Make a transformation

$$\zeta=\begin{pmatrix}\zeta_1\\ \zeta_2\\ \zeta_3\end{pmatrix}=\begin{pmatrix}\omega^2\overline{e}_1\\ \omega\overline{e}_2\\ \overline{e}_3-f_0\end{pmatrix}. \tag{73}$$

Define

$$A_c=\begin{pmatrix}0 & 1\\ -\omega_c^2 & -2\omega_c\end{pmatrix},\quad A_\zeta=\begin{pmatrix}-3\ 1\ 0\\ -3\ 0\ 1\\ -1\ 0\ 0\end{pmatrix}.$$

For A_c, A_ζ are Hurwitz matrixes, so there exist positive matrix P_1 and $\overline{P}_2$, satisfying

$$A_c^{\mathrm{T}}P_1+P_1A_c=-I_2,\quad c_{11}I_2\leq P_1\leq c_{12}I_2 \tag{74}$$

$$A_\zeta^{\mathrm{T}}\overline{P}_2+\overline{P}_2A_\zeta=-I_3,\quad \overline{c}_{21}I_2\leq\overline{P}_2\leq\overline{c}_{22}I_2, \tag{75}$$

where c_{11}, c_{12} are the minimum and maximum eigenvalue of P_1, $\overline{c}_{21}$, $\overline{c}_{22}$ are the minimum and maximum eigenvalue of $\overline{P}_2$. Corresponding to (23), we have

$$P_1 = \begin{pmatrix} \frac{\omega_c^2+5}{4\omega_c} & \frac{1}{2\omega_c^2} \\ \frac{1}{2\omega_c^2} & \frac{\omega_c^2+1}{4\omega_c^3} \end{pmatrix}, \quad \overline{P}_2 = \begin{pmatrix} 1 & -\frac{1}{2} & -1 \\ -\frac{1}{2} & 1 & -\frac{1}{2} \\ -1 & -\frac{1}{2} & 4 \end{pmatrix},$$

$$c_{11} = \frac{1}{8\omega_c^3}\left[\omega_c^4 + 6\omega_c^2 + 1 - \sqrt{(\omega_c^4 + 6\omega_c^2 + 1)(\omega_c^4 + 2\omega_c^2 + 1)}\right], \tag{76}$$

$$c_{12} = \frac{1}{8\omega_c^3}\left[\omega_c^4 + 6\omega_c^2 + 1 + \sqrt{(\omega_c^4 + 6\omega_c^2 + 1)(\omega_c^4 + 2\omega_c^2 + 1)}\right],$$

$$\overline{c}_{21} = 0.1966, \quad \overline{c}_{22} = 4.3372.$$

Define Lyapunov function $V_1(\widetilde{x}) = \widetilde{x}^{\mathrm{T}} P_1 \widetilde{x}$, $\overline{V}_2(\zeta) = \zeta^{\mathrm{T}} \overline{P}_2 \zeta$, and

$$r_1(\omega_c) = 2\sqrt{2}\left(\frac{1}{2\omega_c^2} + \frac{\omega_c^2+1}{4\omega_c^3}\right), \tag{77}$$

$$r_2(\omega_c) = 2\sqrt{\left(\frac{1}{2\omega_c^2}\right)^2 + \left(\frac{\omega_c^2+1}{4\omega_c^3}\right)^2}, \tag{78}$$

$$\overline{s}_1(\omega_c) = 10|\widetilde{a}_1|\sqrt{(2\omega_c)^2 + \omega_c^4}, \tag{79}$$

$$\overline{s}_2 = 10\sqrt{3}|\widetilde{a}_1|, \tag{80}$$

$$\overline{s}_3 = 10|\widetilde{a}_1| \cdot \kappa_2, \tag{81}$$

$$\overline{\rho}_1 = \max\left\{\sqrt{V_1(\widetilde{x}(t_0))},\ 2\sqrt{c_{12}}\left(\frac{\overline{\rho}_2}{\sqrt{\overline{c}_{21}}} r_1(\omega_c) + \kappa_1 r_2(\omega_c)\right)\right\}, \tag{82}$$

$$\overline{\rho}_2 = \max\{\sqrt{\overline{V}_2(\zeta(t_0))},\ (\sqrt{2}+1)\sqrt{\overline{c}_{22}}\kappa_1\}. \tag{83}$$

Likewise, if the parameters ω and ω_c satisfy

$$\omega > \max\left\{2\omega_c, \quad \frac{1}{\kappa_1}\left(\frac{\overline{\rho}_1}{\sqrt{c_{11}}}\overline{s}_1(\omega_c) + \frac{\overline{\rho}_2}{\sqrt{\overline{c}_{22}}}\overline{s}_2 + \overline{s}_3\right)\right\}, \tag{84}$$

then $\|\widetilde{x}\|$, $\|\zeta\|$ are bounded:

$$\|\widetilde{x}\| \le \frac{\overline{\rho}_1}{\sqrt{c_{11}}}, \quad \|\zeta\| \le \frac{\overline{\rho}_2}{\sqrt{\overline{c}_{21}}}. \tag{85}$$

For $\widetilde{x} = \begin{pmatrix} x_1 - x^* \\ x_2 - \dot{x}^* \end{pmatrix}$ and transformation (73), so x, $\widehat{e}$ are bounded.

Make a transformation:

$$\overline{\zeta} = \begin{pmatrix} \overline{\zeta}_1 \\ \overline{\zeta}_2 \\ \overline{\zeta}_3 \end{pmatrix} = \begin{pmatrix} \omega^2 \overline{e}_1 \\ \omega \overline{e}_2 \\ \overline{e}_3 \end{pmatrix}. \tag{86}$$

From (16), (86), we obtain

$$\begin{pmatrix} \dot{\widetilde{x}}_1 \\ \dot{\widetilde{x}}_2 \\ \dot{\overline{\zeta}}_1 \\ \dot{\overline{\zeta}}_2 \\ \dot{\overline{\zeta}}_3 \end{pmatrix} = \begin{pmatrix} 0 & 1 & 0 & 0 & 0 \\ -\omega_c^2 & -2\omega_c & -\omega_c^2/\omega^2 & -2\omega_c/\omega & -1 \\ 0 & 0 & -3\omega & \omega & 0 \\ 0 & 0 & -3\omega & 0 & \omega \\ 0 & 0 & -\omega & 0 & 0 \end{pmatrix} \begin{pmatrix} \widetilde{x}_1 \\ \widetilde{x}_2 \\ \overline{\zeta}_1 \\ \overline{\zeta}_2 \\ \overline{\zeta}_3 \end{pmatrix} + \begin{pmatrix} 0 \\ 0 \\ 0 \\ 0 \\ \eta_4 \end{pmatrix}, \tag{87}$$

where

$$\begin{aligned} \eta_4 = &-\Big(\omega_c^2\widetilde{x}_1 + 2\omega_c\widetilde{x}_2 + \frac{\omega_c^2}{\omega^2}\overline{\zeta}_1 + \frac{2\omega_c}{\omega}\overline{\zeta}_2 + \overline{\zeta}_3\Big)\widetilde{a}_1 \\ &+(\omega_c^2 v + 2\omega_c\dot{v} + \ddot{v} - \omega_c^2 x_1^* - 2\omega_c x_2^*)\widetilde{a}_1 + \dot{f}_0. \end{aligned} \tag{88}$$

Comparing (73) and (86), we get

$$\begin{aligned} \|\overline{\zeta}\| = \sqrt{\overline{\zeta}_1^2 + \overline{\zeta}_2^2 + \overline{\zeta}_3^2} &= \sqrt{\zeta_1^2 + \zeta_2^2 + (\zeta_3 + f_0)^2} \\ &\le \sqrt{2}\cdot\sqrt{\zeta_1^2 + \zeta_2^2 + \zeta_3^2 + f_0^2} \\ &\le \sqrt{2}(\|\zeta\| + |f_0|). \end{aligned}$$

For ζ and f_0 are bounded, and $\|\zeta\| \le \frac{\overline{\rho}_2}{\sqrt{\overline{c}_{21}}}$, $|f_0| \le \kappa_1$, so $\overline{\zeta}$ is bounded. Define

$$\|\overline{\zeta}\| \le \overline{\rho}_3, \quad \overline{\rho}_3 = \sqrt{2}\Big(\frac{\overline{\rho}_2}{\sqrt{\overline{c}_{21}}} + \kappa_1\Big). \tag{89}$$

From (88), η_4 is bounded in the continuous points in f_0. Define $\|\eta_4(t)\| \le \overline{\kappa}_3, t \ne t_i, i = 1, 2, \cdots$, here $\overline{\kappa}_3 = \overline{\kappa}_3(\omega_c, \rho_1, \rho_2, v, \dot{v}, \ddot{v}, A_r, D)$, namely, $\overline{\kappa}_3$ is a constant, which depends on ω_c, the initial values, uncertainty, and the reference signal.

Define $\overline{s}_4 = \sqrt{67}\overline{\kappa}_3$, so similar to the proof of RESO in Step 2, we can prove, when

$$\overline{\omega}_1 = \begin{cases} \max\Big\{\omega\Big|\delta_t = \dfrac{2\overline{c}_{22}\ln\omega}{\omega}\Big\}, & \delta_t \le \dfrac{2\overline{c}_{22}}{e}, \\ 0, & \delta_t > \dfrac{2\overline{c}_{22}}{e}, \end{cases} \tag{90}$$

and then when $\omega > \overline{\omega_1}$, we have

$$\frac{2\overline{c}_{22}\ln\omega}{\omega} < \delta_t. \tag{91}$$

For $i \ge 0$, we have

$$\|\overline{e}\| \le \frac{1}{\omega}\Big(\frac{\overline{c}_{22}}{\overline{c}_{21}}\overline{s}_4 + \frac{\sqrt{\overline{c}_{22}}}{\sqrt{\overline{c}_{21}}}\overline{\rho}_3\Big), \quad t \in [\overline{t}_i^*, t_{i+1}), \tag{92}$$

where

$$\overline{t}_i^* = t_i + \frac{2\overline{c}_{22}\ln\omega}{\omega} < t_{i+1}, \tag{93}$$

and

$$\|\widetilde{x}\| \leq \frac{r_1(\omega_c)}{2c_{11}}\left[\left(\frac{\overline{c}_{22}}{\overline{c}_{21}}\overline{s}_4 + \frac{\sqrt{\overline{c}_{22}}}{\sqrt{\overline{c}_{21}}}H\right)\frac{1}{\omega} + 4\overline{c}_{22}\overline{\rho}_3\frac{\mathrm{e}^{\frac{\delta_t}{2\overline{c}_{12}}}}{1-\mathrm{e}^{-\frac{\delta_t}{2\overline{c}_{12}}}}\cdot\frac{\ln\omega}{\omega}\right], \quad t\in[t_0,\infty). \tag{94}$$

So when $(\frac{\overline{c}_{22}}{\overline{c}_{21}}\overline{s}_4 + \frac{\sqrt{\overline{c}_{22}}}{\sqrt{\overline{c}_{21}}}H)\frac{1}{\omega} \leq 4\overline{c}_{22}\overline{\rho}_3\frac{\mathrm{e}^{\frac{\delta_t}{2\overline{c}_{12}}}}{1-\mathrm{e}^{-\frac{\delta_t}{2\overline{c}_{12}}}}\cdot\frac{\ln\omega}{\omega}$, i.e.,

$$\omega \geq \overline{\omega}_2 = \exp\left(\frac{\frac{\overline{c}_{22}}{\overline{c}_{21}}\overline{s}_4 + \frac{\sqrt{\overline{c}_{22}}}{\sqrt{\overline{c}_{21}}}H}{4\overline{c}_{22}\overline{\rho}_3}\cdot\frac{\mathrm{e}^{\frac{\delta_t}{2c_{12}}}-1}{\mathrm{e}^{\frac{\delta_t}{c_{12}}}}\right), \tag{95}$$

$$\|\widetilde{x}\| \leq \frac{4\overline{c}_{22}\overline{\rho}_3 r_1(\omega_c)}{c_{11}}\cdot\frac{\mathrm{e}^{\frac{\delta_t}{c_{12}}}}{\mathrm{e}^{\frac{\delta_t}{2c_{12}}}-1}\cdot\frac{\ln\omega}{\omega}. \tag{96}$$

Summing up the above (90), (92), (93), (95), (96), we have when

$$\overline{\omega}^* = \max\left\{2\omega_c,\ \frac{1}{\kappa_1}\left(\frac{\overline{\rho}_1}{\sqrt{c_{11}}}\overline{s}_1(\omega_c) + \frac{\overline{\rho}_2}{\sqrt{\overline{c}_{22}}}\overline{s}_2 + \overline{s}_3\right), \overline{\omega}_1, \overline{\omega}_2\right\}, \tag{97}$$

then when $\omega \geq \omega^*$,

$$\|\widehat{e}(t)\| \leq \overline{T}_1\cdot\frac{1}{\omega}, \quad t\in\left[t_{i-1}+2\overline{c}_{22}\frac{\ln\omega}{\omega}, t_i\right), \tag{98}$$

$$\|\widetilde{x}\| \leq \overline{T}_2\cdot\frac{\ln\omega}{\omega}, \quad t\in[t_0,\infty), \tag{99}$$

where

$$\overline{T}_1 = \frac{\overline{c}_{22}}{\overline{c}_{21}}\overline{s}_4 + \frac{\sqrt{\overline{c}_{22}}}{\sqrt{\overline{c}_{21}}}\overline{\rho}_3, \tag{100}$$

$$\overline{T}_2 = \frac{4\overline{c}_{22}\overline{\rho}_3 r_1(\omega_c)}{c_{11}}\cdot\frac{\mathrm{e}^{\frac{\delta_t}{c_{12}}}}{\mathrm{e}^{\frac{\delta_t}{2c_{12}}}-1} \tag{101}$$

are constants which depend on ω_c, initial values, uncertainty, and the reference signals.

Appendix C The Proof of $T_1 \leq \overline{T_1}$ and $T_2 \leq \overline{T_2}$

Comparing (41) with (89), (40) with (83), we have $\overline{\rho}_3 \geq \rho_3$. From (40), (88) and $\|\eta_4(t)\| \leq \overline{\kappa}_3$, $\|\eta_2(t)\| \leq \kappa_3, t \neq t_i, i = 1, 2, \cdots$, we have $\overline{\kappa}_3 > \kappa_3$. Hence, $\overline{s}_4 > s_4$. Because $\overline{c}_{22} > c_{22}$ and $\frac{\overline{c}_{22}}{\overline{c}_{21}} = 22.0610 > \frac{c_{22}}{c_{21}} = 5.8284$, comparing (71) and (100), we have $T_1 \leq \overline{T_1}$.

Besides, for $\overline{\rho}_3 \geq \rho_3$ and $\overline{c}_{22} > c_{22}$, comparing (72) with (101), we have $T_2 \leq \overline{T_2}$.